Quantum and transport lifetimes due to roughness-induced scattering of a two-dimensional electron gas in wurtzite group-III-nitride heterostructures

Doan Nhat Quang
Center for Theoretical Physics, Vietnamese Academy of Science and Technology, P.O. Box 429, Boho, Hanoi 10000, Vietnam

Nguyen Huyen Tung, Vu Ngoc Tuoc, and Nguyen Viet Minh
Institute of Engineering Physics, Hanoi University of Technology, 1 Dai Co Viet Road, Hanoi, Vietnam

Huynh Anh Huy
Department of Physics, School of Education, Cantho University, 3-2 Road, Cantho City, Vietnam

Do Thi Hien
Institute of Physics and Electronics, Vietnamese Academy of Science and Technology, 10 Dao Tan Street, Hanoi, Vietnam
(Received 21 August 2006; published 13 November 2006)

A theory is presented of the quantum and transport lifetimes of the two-dimensional electron gas (2DEG) at low temperature in a uniformly doped wurtzite group-III-nitride single heterostructure. In the calculation, besides the well-known scattering mechanisms, we took into account the roughness-induced scatterings, viz. misfit piezoelectric charges and misfit deformation potential. We proved that these exhibit important scattering sources for the 2DEG in wurtzite group-III-nitride heterostructures, in particular, the piezoelectric charges and alloy disorder dominate the transport and quantum lifetimes in a high-density regime (e.g., $n_s=2\times 10^{12}-10\times 10^{12}$ cm^{-2}). Further, it is found that because of uniform doping, the electron distribution may be remarkably shifted far away from the key scattering sources, thus increasing the lifetimes. Our theory is able to provide a good quantitative explanation of the recent experimental data about the 2DEG lifetimes in a background-doped $Al_xGa_{1-x}N/GaN$ heterostructure. The theory may reproduce not only the magnitude but also the nonmonotonic (bell-shaped) dependencies on the carrier density of both the transport and quantum lifetimes as well as their ratio, which could not be understood if starting merely from the scattering mechanisms known so far.

DOI: 10.1103/PhysRevB.74.205312 PACS number(s): 73.50.Bk, 73.63.Hs, 77.65.Ly

I. INTRODUCTION

In the investigation of transport properties of a two-dimensional electron gas (2DEG) one has recognized a clear distinction between two characteristic relaxation times.[1] The most commonly encountered is the transport lifetime, τ^t. This is defined as an average amount of the intercollision time that an electron remains moving in a particular direction (applied electric field) in the presence of scattering.[2] The transport lifetime can be extracted from the low-field Hall mobility.[3] Another relaxation time is the quantum lifetime, τ^q. This is an average amount of the time that an electron remains in a particular momentum eigenstate in the presence of scattering. The quantum lifetime can be related to disorder-induced broadening of the Landau levels of an electron in a magnetic field,[4] so that this can be extracted from the envelope of the Shubnikov–de Haas oscillations.[5,6]

The transport and quantum lifetimes are important transport parameters used to characterize the performance of high-mobility transistor structures. The improvement of the performance in modern nitride-based devices requires the investigation and identification of detrimental scattering mechanisms. It was shown[2,3,6–12] that one of the most efficient ways to identify them is the study of the evolution of the transport and quantum lifetimes as well as their ratio versus the carrier density.

It is worth mentioning that the above functional dependencies for a 2DEG are determined by some factors, principally, the electronic structure, i.e., its confining sources along the growth direction, and its scattering sources in the in-plane. The latter is specified by the experimental conditions, e.g., the carrier density regime in use. For instance, the quantum lifetime of the 2DEG measured[6] at low (0.3 K) temperature in an $Al_xGa_{1-x}N/GaN$ heterostructure exhibits an increasing function of the density from $n_s=2\times 10^{11}-2\times 10^{12}$ cm^{-2}. This experimental finding suggested[6,10] that charged dislocations may dominate the transport properties of the 2DEG in the $Al_xGa_{1-x}N/GaN$ sample at low densities.

However, Lorenzini *et al.*[11] have just recently reported on the experimental data about the 2DEG in an intentionally undoped single heterostructure made from $Al_{0.23}Ga_{0.77}N$ (210 Å)/GaN (4.7 μm) at high electron densities ($n_s=2\times 10^{12}-10\times 10^{12}$ cm^{-2}). The authors observed the following striking features. First, their transport mobility (and transport lifetime) is much (one order of magnitude) higher than that of a nearly equivalent modulation-doped sample from $Al_{0.25}GA_{0.75}N$ (300 Å)/GaN (0.4 μm) reported in Ref. 12. There, the scattering by remote donors inside of the barrier layer even at a high doping level of 10^{19} cm^{-3} was found not to be responsible for the low mobility, since its individual mobility is two orders higher than the measured one. Thus, the large difference in transport lifetime of the two samples studied in Refs. 11 and 12 still remains unclear.

Second, Lorenzini *et al.*[11] found a discrepancy between the experimental and theoretical values of the quantum lifetime and the lifetime ratio. The measured quantum lifetime

 ©2006 The American Physical Society

shows a pronounced peak in the 2DEG density evolution. This classical bell shape is in contradiction to the prediction from the existing theory[2] based on the traditional scattering sources. In addition, although the measured ratio of the transport to quantum lifetimes has a bell shape as expected from the theory, its peak is, however, two times smaller than the calculated one.

Recently it has been pointed out[13–15] that in actual lattice-mismatched heterostructures interface roughness gives rise to strain fluctuations in both strained and relaxed epilayers. These fluctuations in turn produce random fields: misfit piezoelectric and misfit deformation potentials acting on electrons moving in the in-plane.[14,15] These roughness-induced scatterings are proven[16,17] to be important mechanisms limiting the transport lifetime. So, we will include them in the calculation of the quantum lifetime in wurtzite nitride heterostructures.

Moreover, it should be kept in mind that any doping of the sample affects the 2DEG not only as a scattering source in the in-plane but also a confining source along the growth direction. The modulation doping is intentionally at a high level ($N_{\rm I} \gtrsim 5\times 10^{18}$ cm^{-3}) so that both the effects are to be taken into account. Meanwhile, the background doping is at a low level ($N_{\rm I} \lesssim 5\times 10^{16}$ cm^{-3}), so that this is normally involved merely as a scattering source. Up to now, the confinement effect connected with background doping has hardly been examined. Therefore, a thorough study of this is of obvious interest.

Thus, the goal of the present paper is to develop a theory of the quantum and transport lifetimes of the 2DEG at low temperature in a wurtzite group-III-nitride single heterostructure, taking adequate account of the above-quoted roughness-induced scatterings and the confinement effect arising from background uniform doping.

The paper is organized as follows. In Sec. II below, for calculation of the electronic structure we derive the potentials due to all possible confining sources. In Sec. III, we supply the basic equations to calculate the transport and quantum lifetimes due to different scattering mechanisms. Section IV is devoted to numerical results and conclusions with reference to recent experiments on the lifetimes at high carrier densities. Finally, a summary is given in Sec. V.

II. 2DEG IN A UNIFORMLY DOPED WURTZITE NITRIDE HETEROSTRUCTURE

A. Variational wave function for the 2DEG in a heterostructure of finite depth

We will be dealing with wurtzite group-III-nitride single heterostructures, e.g., an $Al_xGa_{1-x}N/GaN$ sample, which is composed of an $Al_xGa_{1-x}N$ layer grown pseudomorphically on a GaN layer. The crystal reference system is such that the z axis is opposite to the growth direction [0001], and $z=0$ defines the interface plane between the $Al_xGa_{1-x}N$ barrier ($z<0$) and the GaN well ($z>0$). It is assumed that the $Al_xGa_{1-x}N$ layer be under tensile strain, while the GaN layer be relaxed.

As usual,[18,19] for the electrons confined in the channel we assume a triangular quantum well (QW) located along the growth direction. It was indicated[20–23] that the potential barrier height may play an important role in certain phenomena. Therefore, we must in general adopt the realistic model of finitely deep wells.

At low temperature, the 2DEG is assumed to primarily occupy the lowest subband. It has been shown[20–22] that for a finitely deep triangular QW, this may be very well described by a modified Fang-Howard wave function, proposed by Ando,[20]

$$\zeta(z) = \begin{cases} A\kappa^{1/2}\exp(\kappa z/2), & \text{for } z<0, \\ Bk^{1/2}(kz+c)\exp(-kz/2), & \text{for } z>0, \end{cases} \tag{1}$$

in which A, B, c, k, and κ are variational parameters to be determined. Here k and κ are half the wave numbers in the well and the barrier, respectively. A, B, and c are dimensionless parameters given in terms of k and κ through the boundary conditions at the interface plane $z=0$ and the normalization. These read as[21,22]

$$A\kappa^{1/2} = Bk^{1/2}c,$$

$$A\kappa^{3/2}/2 = Bk^{3/2}(1-c/2),$$

$$A^2 + B^2(c^2+2c+2) = 1. \tag{2}$$

.

The wave function of the lowest subband is to minimize the total energy per electron, which is determined by the Hamiltonian:

$$H = T + V_{\rm tot}(z), \tag{3}$$

where T is the kinetic energy and $V_{\rm tot}(z)$ is the effective confining potential. The latter arises from all possible confining sources located along the growth direction, viz. potential barrier, polarization charges on the interface, Hartree potential created by ionized donors and 2DEG, and exchange-correlation corrections,

$$V_{\rm tot}(z) = V_{\rm b}(z) + V_\sigma(z) + V_{\rm H}(z) + V_{\rm xc}(z). \tag{4}$$

The last term allows for a many-body effect in the 2DEG, which may be of some importance at high carrier densities.

B. Confining potentials in a uniformly doped heterostructure

Thus, in order to determine the QW wave function of interest, we have to specify the individual confining potentials appearing in Eq. (4).

First, the potential barrier of some finite height V_0 located at the interface plane $z=0$ yields

$$V_{\rm b}(z) = V_0\theta(-z), \tag{5}$$

with $\theta(z)$ as a unity step function. The barrier height is related to the conduction band offset between the $Al_xGa_{1-x}N$ and GaN layers.

It is well known[24–26] that due to piezoelectric and spontaneous polarizations in strained nitride heterostructures there exist positive bound charges localized on the interface. The polarization charges create a normal uniform electric field, given by

$$V_\sigma(z) = \frac{2\pi}{\varepsilon_L} e\sigma|z|, \tag{6}$$

with σ as their total sheet density. Here ε_L is the dielectric constant of the sample, neglecting a small difference in its values between the well and barrier layers with the use of an average value.

It was found[27] that the total density of polarization charges is large ($\sigma/e \gtrsim 10^{12}$ cm^{-2}), so their electric field is strong ($\gtrsim 10^6$ V/cm). This facilitates the electron transfer from localized donor states or, in case of very strong fields, possibly even from the valance band to the QW at the interface. It was assumed[28] that this enables a density of unintentional ionized donors of 5×10^{16} cm^{-3} in the whole sample.

Next, we are dealing with the Hartree potential induced by the ionized donors and the electron distribution in the QW. This is determined according to Poisson's equation[22,29]

$$\frac{d^2}{dz^2} V_H(z) = \frac{4\pi e^2}{\varepsilon_L}[N_I(z) - n(z)], \tag{7}$$

in which $N_I(z)$ is the bulk density of impurities (per unit volume) varying along the growth direction, and $n(z)$ the electron density.

The sample is uniformly doped, either intentionally in some space at a high doping level (e.g., $N_I \gtrsim 5\times10^{18}$ cm^{-3}), or unintentionally (background) in its whole space at a low one ($N_I \lesssim 5\times10^{16}$ cm^{-3}). Accordingly, the sample is assumed to be doped with a constant impurity density N_I in a region surrounding the 2DEG and spreading from $-z_b$ in the barrier to z_w in the well: $z_b \leqslant L_b$ and $z_w \leqslant L_w$, with L_b and L_w as their thicknesses, so

$$N_I(z) = \begin{cases} N_I, & \text{for } -z_b \leqslant z \leqslant z_w, \\ 0, & \text{elsewhere}. \end{cases} \tag{8}$$

The electron density distribution along the z axis is fixed by the envelope wave function from Eq. (1):

$$n(z) = n_s|\zeta(z)|^2, \tag{9}$$

with n_s as a sheet density of the 2DEG.

We solve Poisson's equation (7) in combination with electrostatic boundary conditions, especially the vanishing of the electric field at infinity $z\to\pm\infty$.[29] As a result, we may arrive at an analytic expression for the Hartree potential,

$$V_H(z) = \frac{4\pi e^2}{\varepsilon_L}\begin{cases} -N_I z_b^2/2 - n_s f(z), \\ N_I z(z+2z_b)/2 - n_s f(z), \\ N_I z(z-2z_w)/2 - n_s[g(z)-g(0)+f(0)], \\ -N_I z_w^2/2 - n_s[g(z)-g(0)+f(0)], \end{cases} \tag{10}$$

in which the z intervals are, respectively, such that $z<-z_b$, $-z_b<z<0$, $0<z<z_w$, and $z>z_w$.

The functions figuring in Eq. (10) are defined in terms of the variational parameters entering the electron wave function, given by

$$f(z) = A^2\frac{e^{\kappa z}}{\kappa} \tag{11}$$

and

$$g(z) = B^2 e^{-kz}\left[kz^2 + 2(c+2)z + \frac{c^2+4c+6}{k}\right]. \tag{12}$$

It is readily seen from Eq. (10) that within the variational approximation with the use of the wave function from Eq. (1), the Hartree potential may be separated into two parts:

$$V_H(z) = V_I(z) + V_s(z). \tag{13}$$

The first term is to be regarded as the impurity potential fixed by the doping profile, viz. the impurity density N_I and the doping sizes z_w, z_b; while the second one as the 2DEG potential fixed by the sheet electron density n_s and their distribution, i.e., the variational parameters.

At last, the exchange-correlation corrections allow for the many-body effect in the 2DEG, given by[30,31]

$$V_{xc}(z) = -0.611\frac{e^2}{\varepsilon_L}\left[\frac{3}{4\pi}n(z)\right]^{1/3}, \tag{14}$$

with $n(z)$ as the electron distribution from Eq. (9).

C. Total energy per electron in the lowest subband

We now turn to the total energy per electron for the 2DEG occupying the ground-state subband. The expectation value of the Hamiltonian from Eqs. (3) and (4) reads as

$$E_0(k,\kappa) = \langle T\rangle + \langle V_b\rangle + \langle V_\sigma\rangle + \langle V_I\rangle + \langle V_s\rangle + \langle V_{xc}\rangle. \tag{15}$$

Upon employing the above-derived analytic expressions for the individual confining potentials, we easily estimate their expectation values for an electron described by the wave function from Eq. (1). The average energies figuring in Eq. (15) are supplied in the following.

For the kinetic energy, it holds

$$\langle T\rangle = -\frac{\hbar^2}{8m_z}[A^2\kappa^2 + B^2k^2(c^2-2c-2)], \tag{16}$$

where m_z is the effective electron mass of GaN in the growth direction.

For the potentials related to the barrier and polarization charges located on the interface, we have

$$\langle V_b\rangle = V_0 A^2 \tag{17}$$

and

$$\langle V_\sigma\rangle = \frac{2\pi e\sigma}{\varepsilon_L}\left[\frac{A^2}{\kappa} + \frac{B^2}{k}(c^2+4c+6)\right]. \tag{18}$$

Next, the average potential due to charged impurities can be written in terms of the dimensionless doping sizes, $u = kz_w$ and $v = \kappa z_b$, by

$$\langle V_{\rm I}\rangle = -\frac{4\pi e^2 N_{\rm I}}{\varepsilon_{\rm L}}\Bigg\{A^2 z_{\rm b}^2\left[\frac{e^{-v}}{2} - h_2(v) + v h_1(v)\right] - B^2 z_{\rm w}^2\Bigg[12h_4(u) + 6(c-u)h_3(u) + c(c-4u)h_2(u) - c^2 u h_1(u) - \frac{e^{-u}}{2}[u^2 + 2(c+1)u + c^2 + 2c + 2]\Bigg]\Bigg\}, \qquad (19)$$

where we introduced an auxiliary function

$$h_n(x) = \frac{1}{x^2}\left(1 - e^{-x}\sum_{l=0}^{n}\frac{x^l}{l!}\right), \qquad (20)$$

with $n=0,1,2,\ldots$ as an integer.

In the case of experimental interest,[3,11,12] the doping sizes are usually large enough so that u, $v \gg 1$. Then, by adopting the approximation $h_n(x) \approx 1/x^2$ for $x \gg 1$, Eq. (19) is simplified to

$$\langle V_{\rm I}\rangle = \frac{4\pi e^2 N_{\rm I}}{\varepsilon_{\rm L}}\left[\frac{A^2}{\kappa} z_{\rm b} - \frac{B^2}{k} z_{\rm w}(c^2 + 4c + 6)\right]. \qquad (21)$$

Lastly, for the 2DEG and exchange-correlation potentials, it holds

$$\langle V_{\rm s}\rangle = \frac{4\pi e^2 n_{\rm s}}{\varepsilon_{\rm L}}\left[\frac{A^4}{2\kappa} - \frac{A^2}{\kappa} + \frac{B^4}{4k}(2c^4 + 12c^3 + 34c^2 + 50c + 33)\right] \qquad (22)$$

and

$$\langle V_{\rm xc}\rangle = -0.611\frac{e^2}{\varepsilon_{\rm L}}\left(\frac{3}{4\pi}n_{\rm s}\right)^{1/3}\left[\frac{3}{4}A^{8/3}\kappa^{1/3} + \left(\frac{3}{4}\right)^{11/3} B^{8/3}k^{1/3}e^{4c/3}\Gamma\left(\frac{11}{3},\frac{4c}{3}\right)\right], \qquad (23)$$

with $\Gamma(a,x)$ as an incomplete Gamma function.[32]

D. Infinitely high potential barrier

To illustrate the effect of uniform doping on quantum confinement of the 2DEG, we examine a QW of infinite depth ($V_0 \to \infty$). In this limiting case, we have $A=0$, $B=1/\sqrt{2}$, $c=0$, so that Eq. (21) is simplified to

$$\langle V_{\rm I}\rangle = -\frac{12\pi e^2}{\varepsilon_{\rm L}}\frac{N_{\rm I} z_{\rm w}}{k}. \qquad (24)$$

The centroid of the electron distribution along the growth direction is known[18] to be located at

$$z_0 = 3/k, \qquad (25)$$

from which its size is accordingly estimated to be $2z_0$.

The total energy per electron is supplied by a modification of Eq. (15), where the average 2DEG energy $\langle V_{\rm s}\rangle$ is to be replaced with its half.[18,21,22] Moreover, for simplicity the exchange-correlation corrections are omitted. Then, as a result of the minimization of the total energy per electron with respect to the well wave vector k, we obtain

$$k = \left\{\frac{48\pi m_z e^2}{\hbar^2 \varepsilon_{\rm L}}\left[\frac{11}{32}n_{\rm s} + \frac{1}{2}\frac{\sigma}{e} - N_{\rm I} z_{\rm w}\right]\right\}^{1/3}. \qquad (26)$$

This expression for k is clearly distinguished from the earlier formula[17,18] by the presence of the last term on the right-hand side, $N_{\rm I} z_{\rm w}$, which is referred to as the doping capacity. It is observed from Eqs. (25) and (26) that the electron distribution is shaped not only by the densities of electrons and polarization charges but also that of ionized donors. Since the charged donors decrease the well wave vector, they increase the centroid of the 2DEG and, hence, its size. Therefore, the 2DEG is shifted in the direction from the barrier to the well layers, i.e., far away from such scattering sources that are located in the barrier or near the interface, e.g., alloy disorder, surface roughness, misfit piezoelectric charges, and misfit deformation potential. This means that a uniform doping of the well layer can lead to a weakening of scatterings, and an enhancement of the transport and quantum lifetimes.

In the actual model of finitely deep QWs, the attractions of the 2DEG by charged donors in the well and in the barrier are counteracting, as seen from Eq. (21). However, since the former is usually much (more than one order) longer than the latter,[3,11,12] the 2DEG is shifted toward the well side, so the lifetimes are raised as above.

III. LOW-TEMPERATURE TRANSPORT AND QUANTUM LIFETIMES

A. Basic equations

In this section we are dealing with the transport properties of the 2DEG at high density and low temperature in wurtzite group-III-nitride heterostructures, e.g., made from $\mathrm{Al}_x\mathrm{Ga}_{1-x}\mathrm{N}/\mathrm{GaN}$. For this purpose, we gather basic equations necessary for calculation of the relaxation times.

The electrons moving along the in-plane are scattered by different disorder sources, which are normally characterized by some random fields. Scattering by a Gaussian random field is specified by its autocorrelation function in wave vector space $\langle|U(\mathbf{q})|^2\rangle$.[18] Hereafter, $U(\mathbf{q})$ is a 2D Fourier transform of the unscreened potential weighted with the lowest-subband wave function from Eq. (1):

$$U(\mathbf{q}) = \int_{-\infty}^{+\infty} dz|\zeta(z)|^2 U(\mathbf{q},z). \qquad (27)$$

In a high-density regime ($n_{\rm s} \gtrsim 10^{12}\ \mathrm{cm}^{-2}$) the multiple scattering effects are negligibly small,[33] so that we may adopt the linear transport theory as a good approximation. The inverse transport and quantum lifetimes for low (zero) temperature are then represented in terms of the autocorrelation function for each disorder as follows:[1,34,35]

$$\frac{1}{\tau^{\rm t}} = \frac{1}{2\pi\hbar E_{\rm F}}\int_0^{2k_{\rm F}} dq\frac{q^2}{(4k_{\rm F}^2 - q^2)^{1/2}}\frac{\langle|U(\mathbf{q})|^2\rangle}{\varepsilon^2(q)} \qquad (28)$$

and

$$\frac{1}{\tau^{\mathrm{q}}} = \frac{1}{2\pi\hbar E_{\mathrm{F}}}\int_0^{2k_{\mathrm{F}}} dq \frac{2k_{\mathrm{F}}^2}{(4k_{\mathrm{F}}^2 - q^2)^{1/2}} \frac{\langle |U(\mathbf{q})|^2\rangle}{\varepsilon^2(q)}. \quad (29)$$

Here $\mathbf{q}$ denotes the momentum transfer by a scattering event in the interface plane, $q=|\mathbf{q}|=2k_{\mathrm{F}}\sin(\theta/2)$ with θ as an angle of scattering. The Fermi wave number is fixed by the sheet electron density: $k_{\mathrm{F}}=\sqrt{2\pi n_{\mathrm{s}}}$ and $E_{\mathrm{F}}=\hbar^2 k_{\mathrm{F}}^2/2m^*$, with m^* as the effective electron mass of GaN in this plane.

The dielectric function $\varepsilon(q)$ entering Eqs. (28) and (29) allows for the screening of the scattering potentials by the 2DEG. As usual, this is evaluated within the random phase approximation[18,22]

$$\varepsilon(q) = 1 + \frac{q_{\mathrm{s}}}{q} F_{\mathrm{S}}(q/k)[1 - G(q/k)], \quad \text{for } q \leqslant 2k_{\mathrm{F}}, \quad (30)$$

with $q_{\mathrm{s}}=2m^* e^2/\varepsilon_{\mathrm{L}}\hbar^2$ as the inverse two-dimensional (2D) Thomas-Fermi screening length. The screening form factor $F_{\mathrm{S}}(t)$ depends on the electron distribution, i.e., the envelope wave function from Eq. (1). For instance, it holds for the limiting case of infinitely deep QWs,[18]

$$F_{\mathrm{S}}(t) = \frac{3t^2 + 9t + 8}{8(t+1)^3}, \quad (31)$$

with $t=q/k$ as the dimensionless in-plane wave vector and k the well wave vector. The local field corrections are due to the many-body exchange effect in the in-plane, given by[36]

$$G(t) = \frac{t}{2(t^2 + t_{\mathrm{F}}^2)^{1/2}}, \quad \text{with } t_{\mathrm{F}} = k_{\mathrm{F}}/k. \quad (32)$$

Next, we outline the possible scattering mechanisms for uniformly doped wurtzite group-III-nitride heterostructures at very low temperature, namely the one studied in Ref. 11. The sample was intentionally undoped, so that it is assumed to be subjected to some uniform residual (background) doping. The phonon scattering is evidently negligibly weak. In addition, we omit the scattering by charged dislocations since with an inclusion of their interactions the dislocation scattering is seemingly less important in limiting the measured relaxation times. Therefore, the electrons are expected to experience the following scattering mechanisms: (i) background impurities (BI), (ii) alloy disorder (AD), (iii) surface roughness (SR), (iv) misfit piezoelectric charges (PE), and (v) misfit deformation potential (DP). The overall (transport or quantum) lifetime is then determined by the ones for individual disorders according to Matthiessen's rule

$$\frac{1}{\tau_{\mathrm{tot}}} = \frac{1}{\tau_{\mathrm{BI}}} + \frac{1}{\tau_{\mathrm{AD}}} + \frac{1}{\tau_{\mathrm{SR}}} + \frac{1}{\tau_{\mathrm{PE}}} + \frac{1}{\tau_{\mathrm{DP}}}. \quad (33)$$

B. Autocorrelation functions for scattering mechanisms

1. Background impurity

As clearly seen from Eqs. (28) and (29), in our calculation of the relaxation times the autocorrelations functions in wave vector space $\langle |U(\mathbf{q})|^2\rangle$ take a key role. Thus, we ought to specify them for the above-mentioned scattering sources. Some of them have already been derived in our previous work[16] for modulation-doped samples. So, in what follows we will list them and give the modifications necessary for uniformly doped systems.

We are now dealing with the scattering by background impurities, assuming an infinitely deep triangular QW. This seems to be a good approximation for the special case of uniform doping, where the 2DEG is surrounded by the impurities. In accordance with experimental conditions,[3,11,12,37] the doping regions in the well and barrier layers are to be regarded as infinitely long.[37] Moreover, the sample is subjected to thermal treatment during epitaxial growth. Therefore, one has to allow for high-temperature ionic correlation[38,39] because Coulomb interactions between the charged impurities in diffusion tend to diminish the probability for large fluctuations in their density. Consequently, the correlation among impurities reduces the quantities averaged over their configurations, e.g., their autocorrelation function.[40,41] This means that ionic correlation weakens the impurity scattering, so that the respective individual lifetimes can be increased significantly, e.g., up to one order of magnitude as in the case of modulation doping.[17]

As a result, we may derive the autocorrelation function for background doping of the whole sample in the following form:[17,41,42]

$$\langle |U_{\mathrm{BI}}(\mathbf{q})|^2\rangle_{\mathrm{c}} = \left(\frac{2\pi e^2}{\varepsilon_{\mathrm{L}}}\right)^2 \frac{N_{\mathrm{I}}}{2k^3} F_{\mathrm{BI}}^{\mathrm{uns}}(q/k), \quad (34)$$

where $\langle \ldots \rangle_{\mathrm{c}}$ stands for the averaging over a correlated impurity distribution, N_{I} is their bulk density. Here, the form factor for unscreened background-impurity scattering is defined by

$$F_{\mathrm{BI}}^{\mathrm{uns}}(t) = \frac{1}{t^2(t+t_{\mathrm{c}})}[d_1(t) - 12d_2(t) - 4d_3(t) + 6d_4(t) + d_5(t) - d_5(-t)]. \quad (35)$$

The functions figuring in Eq. (35) are given by

$$d_1(t) = \frac{1}{(t-1)^6},$$

$$d_2(t) = \frac{t}{(t+1)^4(t-1)^3},$$

$$d_3(t) = \frac{t}{(t+1)^2(t-1)^6}\left[2 + \frac{(t-1)^2}{t+1}\right],$$

$$d_4(t) = \frac{t}{(t^2-1)^3}\left[1 - \frac{t^2-1}{4} + \frac{(t^2-1)^2}{8}\right],$$

$$d_5(t) = \frac{t}{(t+1)^6}\left[2 + t + (t+1)^2 + \frac{3(t+1)^3}{4} + \frac{3(t+1)^4}{8}\right]. \quad (36)$$

We introduced in Eq. (35) a dimensionless parameter which quantifies the ionic correlation effect:

$$t_c = \frac{2\pi e^2 n_I}{\varepsilon_L k_B T_0} \frac{1}{k}, \quad (37)$$

with n_I as the sheet impurity density, given by[38] $n_I = N_I^{2/3}$, T_0 as the freezing temperature for impurity diffusion ($\sim$1000 K), and k_B the Boltzmann constant.

It should be stressed that the ionic correlation is of great importance in the linear transport theory. Indeed, an inspection of Eqs. (34)–(36) reveals the following asymptotic behavior of the autocorrelation function for correlated impurities at $q \to 0$ (i.e., forward scattering $\theta \to 0$): $\langle |U_{BI}(\mathbf{q})|^2 \rangle_c \sim 1/q^2$. This enables the integral for the quantum lifetime given by Eq. (29) convergent since from Eq. (30): $\varepsilon(q) \sim 1/q$. On the contrary, for random impurities ($t_c = 0$): $\langle |U_{BI}(\mathbf{q})|^2 \rangle_r \sim 1/q^3$, so the relevant integral is logarithmically divergent (cf. the case of square QWs[35,43]). Therefore, in the previous theories of the quantum lifetime one has to claim the multiple-scattering events[43] or a scattering angle cutoff θ_c as an empirical prescription.[44]

It is interesting to note that such a divergence was also met in the calculation of the quantum lifetime due to charged dislocations, so that one has to invoke a scattering angle cutoff θ_c.[10] It is known[6,43,45] that this cutoff is connected with the multiple scattering events. The quantum lifetime thus obtained turns out to drastically depend on the value of θ_c in choice. On the other hand, the interactions between the dislocations are known to be important, e.g., these result in an enhanced critical thickness of the strained layer in a lattice-mismatched structure.[46] From the above result for correlated impurities, we argue that the quantum lifetime due to charged dislocations might become convergent if their interactions are included in the calculation. In other words, we suggest that the interactions among dislocations can lead to a remarkable reduction of scattering by them.

2. Alloy disorder

Next, we are concerned with scattering of the confined electrons in the Ga channel by alloy disorder located in the $Al_xGa_{1-x}N$ barrier. Hereafter, we again work within the realistic model of finitely deep QWs. It is known[27] that the structure under study has the Ga(Al)-faced polarity. Accordingly, the alloy disorder must begin with the first (nearest to the interface) layer composed of randomly arranged Ga and Al atoms rather than the one of N atoms only.[27,47] In other words, the region of the alloy interaction spreads actually from $-L_b$ to $-L_a$, with L_b as the thickness of the barrier layer, and $L_a \sim 3.3$ Å as the distance from the first Ga(Al) layer to the interface.[23,27,47,48]

Thus, the autocorrelation function for alloy scattering is correctly provided by[20,21]

$$\langle |U_{AD}(\mathbf{q})|^2 \rangle = x(1-x) u_{al}^2 \Omega \int_{-L_b}^{-L_a} dz \zeta^4(z). \quad (38)$$

Here, x is the Al content of the alloy layer, and u_{al} is the alloy potential assumed[21] to be close to the conduction band offset between AlN and GaN: $u_{al} \approx \Delta E_c(1) = 2.03$ eV. The volume of a hexagonal unit cell is given by[29] $\Omega = \sqrt{3} a^2(x) c(x)/2$, with $a(x)$ and $c(x)$ as the lattice constants of the alloy.

By means of Eq. (1) for the lowest-subband wave function, the autocorrelation function in question is written in terms of the barrier wave number κ as follows:

$$\langle |U_{AD}(\mathbf{q})|^2 \rangle = x(1-x) u_{al}^2 \Omega \frac{A^4 \kappa}{2} [e^{-2\kappa L_a} - e^{-2\kappa L_b}]. \quad (39)$$

Thus, different from the previous theory,[17,21] the first term in the square brackets on the right-hand side of Eq. (39) is seen as less than unity. This leads to a remarkable reduction of the alloy scattering in the case of Ga(Al)-faced polarity. The effect is important, in particular, for high-mobility systems, where the alloy interaction is with the tail of the electron distribution in the barrier. It is to be noticed that to explain a measured high individual mobility due to alloy disorder, one has to recently claim the alloy potential as smaller than the above-quoted conduction band offset: $u_{al} = 1.8$ (Refs. 49 and 50) and 1.5 eV.[51]

3. Surface roughness

We turn to the treatment of 2DEG scattering mechanisms which originate from interface roughness, namely surface roughness, misfit piezoelectric charges, and misfit deformation potential. The first one is a traditional scattering source, which is due to roughness-induced fluctuations in the position of the potential barrier. The weighted scattering potential in wave vector space is fixed by the value of the envelope wave function at the interface plane, given by[18]

$$U_{SR}(\mathbf{q}) = V_0 |\zeta(0)|^2 \Delta_{\mathbf{q}}, \quad (40)$$

where V_0 is the potential barrier height, and $\Delta_{\mathbf{q}}$ denotes a Fourier transform of the interface roughness profile.

As has been dramatically warned in Ref. 18, the use of the local value of the variational wave function at a single point, e.g., $z=0$, can lead to serious errors in the calculation of surface roughness scattering. Therefore, in difference from the earlier theory,[52,53] we need to establish a formula for the autocorrelation function of interest in terms of some integral quantities involving the trial wave function on the whole z axis.

For this purpose we adopt the following relationship, valid for any bound electronic state:[16,54]

$$\int_{-\infty}^{+\infty} dz |\zeta(z)|^2 \frac{\partial V_{tot}(z)}{\partial z} = 0, \quad (41)$$

which is exact and applicable for any value of the barrier height V_0. Thus by replacing the effective confining potential with Eq. (4), we may represent the local value of the wave function via the expectation values of the electric fields created by the individual confining sources,

$$V_0 |\zeta(0)|^2 = \langle V'_\sigma \rangle + \langle V'_I \rangle + \langle V'_s \rangle + \langle V'_{xc} \rangle, \quad (42)$$

with $V' = \partial V(z)/\partial z$.

Next, by putting Eq. (42) into Eq. (40), we arrive at the autocorrelation function for surface roughness:

$$\langle |U_{SR}(\mathbf{q})|^2 \rangle = |\langle V'_\sigma \rangle + \langle V'_I \rangle + \langle V'_s \rangle + \langle V'_{xc} \rangle|^2 \langle |\Delta_{\mathbf{q}}|^2 \rangle. \quad (43)$$

Thus, we must evaluate the average electric fields appearing in Eqs. (43). The calculation is straightforward by means of

the lowest-subband wave function from Eq. (1). The result reads as follows.

For polarization charges of sheet density σ,

$$\langle V'_\sigma \rangle = \frac{4\pi e^2}{\varepsilon_L}\frac{\sigma}{2e}(1-2A^2). \tag{44}$$

For uniform doping of bulk impurity density N_I,

$$\langle V'_I \rangle = \frac{4\pi e^2}{\varepsilon_L} N_I \left\{ \frac{A^2 v}{\kappa}[1 - v h_0(v)] + \frac{B^2 u^2}{k}[6h_3(u) + 2(2c-u)h_2(u) + c(c-2u)h_1(u) - c^2 u h_0(u)] \right\}, \tag{45}$$

which is, for large doping sizes, simplified to

$$\langle V'_I \rangle = \frac{4\pi e^2}{\varepsilon_L} N_I [A^2 z_b - 2B^2 z_w (c+1)]. \tag{46}$$

For the 2DEG distribution of sheet density n_s,

$$\langle V'_s \rangle = -\frac{4\pi e^2}{\varepsilon_L}\frac{n_s}{2}\{A^4 - B^4[c(c+2)+2]^2\}. \tag{47}$$

Last, for exchange-correlation corrections,

$$\langle V'_{xc} \rangle = -0.611\frac{e^2}{\varepsilon_L}\left(\frac{3}{4\pi}n_s\right)^{1/3}\left\{\frac{A^{8/3}}{4}\kappa^{4/3} + \frac{B^{8/3}}{3}k^{4/3} \times \left[\left(\frac{3}{4}\right)^{8/3} e^{4c/3}\Gamma\left(\frac{8}{3},\frac{4c}{3}\right) - c^{11/3}\Psi\left(2,\frac{14}{3};\frac{4c}{3}\right)\right]\right\}, \tag{48}$$

where $\Psi(a,c;x)$ is a confluent hypergeometric function.[32]

In the limiting case of infinitely deep QWs ($V_0 \to \infty$) and neglecting the exchange-correlation corrections, Eq. (43) yields a simple autocorrelation function:

$$\langle |U_{SR}(\mathbf{q})|^2 \rangle = \left(\frac{4\pi e^2}{\varepsilon_L}\right)^2\left(\frac{1}{2}n_s + \frac{1}{2}\frac{\sigma}{e} - N_I z_w\right)^2 \langle |\Delta_\mathbf{q}|^2 \rangle. \tag{49}$$

It is clearly seen from Eq. (49) that the last term on the right-hand side describes the effect from uniform doping on surface roughness scattering. This weakens the scattering and shows up in a quadratic dependence on the doping capacity, i.e., the impurity density and the well doping size.

It follows from Eqs. (43) and (49) that surface roughness scattering depends strongly on the interface profile. This is well described by a power-law distribution,[13,55] which can be written in terms of the dimensionless in-plane wave vector $t=q/k$, with k as the well wave vector, as follows:

$$\langle |\Delta_\mathbf{q}|^2 \rangle = \pi \Delta^2 \Lambda^2 F_{SR}^{uns}(q/k), \tag{50}$$

where Δ is a roughness amplitude and Λ is a correlation length. The form factor for unscreened surface roughness scattering is given by

$$F_{SR}^{uns}(t) = \frac{1}{[1+(\Lambda k)^2 t^2/4n]^{n+1}}, \tag{51}$$

where n is an exponent fixing the falloff of the distribution at large in-plane wave numbers. Thus, the interface profile is specified by the falloff exponent n and the dimensionless correlation length Λk. For rather smooth interfaces, we will take a large exponent $n=4$. The correlation length Λ is chosen as an adjustable parameter for fitting to the experiment under study.

4. Misfit piezoelectric charges

As already mentioned before, in lattice-mismatched epilayered structures, surface roughness gives rise to strain fluctuations in both strained and relaxed layers.[13–15] In a wurtzite nitride heterostructure made, e.g., from $Al_xGa_{1-x}N/GaN$ these induce fluctuating densities of piezoelectric charges, viz. bulk charges inside of the strained and relaxed layers as well as sheet charges on the interface.[15] The charges create relevant random electric fields and act as scattering sources on the motion of electrons in the in-plane.[17]

The impact on the 2DEG from the piezoelectric field due to charges in the well is found to be much stronger than that due to charges in the barrier and on the interface.[15] Therefore, we may restrict the calculation to the scattering by charges located inside of the well. Then, by means of the lowest-subband wave function from Eq. (1) the autocorrelation function for roughness-induced misfit piezoelectric charges is supplied by[17]

$$\langle |U_{PE}(\mathbf{q})|^2 \rangle = \left[\frac{\pi^{3/2}\alpha\epsilon_\parallel e Q \Delta\Lambda}{\varepsilon_L}\right]^2 F_{PE}^{uns}(q/k), \tag{52}$$

where $\epsilon_\parallel$ is the lattice mismatch, and α denotes the anisotropy ratio as a measure for the deviation of hexagonal symmetry of the wurtzite crystal from isotropy ($\alpha \sim 5$).

We introduced a material parameter characteristic of the well, defined in terms of its elastic stiffness c_{ij}^w and piezoelectric e_{ij}^w constants by

$$Q = \frac{C_b}{c_{33}^b}\left[\frac{e_{15}^w}{c_{44}^w} + \frac{e_{31}^w(c_{33}^w + 2c_{13}^w) - e_{33}^w(c_{11}^w + c_{12}^w + c_{13}^w)}{C_w}\right], \tag{53}$$

where

$$C_\lambda = c_{33}^\lambda(c_{11}^\lambda + c_{12}^\lambda) - 2(c_{13}^\lambda)^2, \tag{54}$$

with $\lambda = w$, b as the labels for the well and barrier layers, respectively.

The form factor entering in Eq. (52) is characteristic of the unscreened misfit piezoelectric scattering, given by

$$F_{PE}^{uns}(t) = F_{SR}^{uns}(t)\left[\frac{A^2 a}{2(t+a)} + \frac{B^2}{2(t+1)}\left\{\frac{2}{(t+1)^2} + \frac{2c}{t+1} + c^2 + \frac{2t}{t+1}\left(\frac{6}{(t+1)^2} + \frac{4c}{t+1} + c^2\right)\right\}\right]^2, \tag{55}$$

where $F_{SR}^{uns}(t)$ is yielded by Eq. (51), $a=\kappa/k$; A, B, and c are the variational parameters of the wave function. In the limiting case of $V_0 \to \infty$, this is simplified to

$$F_{\rm PE}^{\rm uns}(t) = \frac{F_{\rm SR}^{\rm uns}(t)}{(t+1)^6}\left(\frac{3t}{t+1} + \frac{1}{2}\right)^2. \quad (56)$$

5. Misfit deformation potential

Further, strain fluctuations also induce nonuniform shifts of the band edges. This implies that electrons in the conduction band and holes in the valence one must experience a random perturbating potential. The roughness-induced misfit deformation potentials exist in both the well and barrier layers and decays exponentially far away from the interface.[13,14,17] Since the 2DEG is located mainly in the well, we can thus take into account the scattering merely in this layer.

As a result, by means of the wave function from Eq. (1) we may find the following autocorrelation function for the unscreened misfit deformation potential[17]

$$\langle |U_{\rm DP}(\mathbf{q})|^2\rangle = \left[\frac{\pi^{1/2}\alpha\epsilon_{\parallel}\Xi_{\rm d}\Delta\Lambda}{2}\frac{C_{\rm b}}{c_{33}^{\rm b}}\frac{c_{11}^{\rm w}+c_{12}^{\rm w}+c_{13}^{\rm w}}{C_{\rm w}}\right]^2 \times k^2 F_{\rm DP}^{\rm uns}(q/k), \quad (57)$$

where $\Xi_{\rm d}$ is the combined dilational component of the deformation potential for the conduction band.[56,57] As a lower bound for this coupling constant, we may assume[17] $\Xi_{\rm d} = 22.57$ eV.

The form factor in Eq. (57) is defined by

$$F_{\rm DP}^{\rm uns}(t) = F_{\rm SR}^{\rm uns}(t)\left(\frac{B^2 t}{t+1}\right)^2\left[\frac{2}{(t+1)^2} + \frac{2c}{t+1} + c^2\right]^2, \quad (58)$$

which for $V_0 \to \infty$ yields

$$F_{\rm DP}^{\rm uns}(t) = \frac{F_{\rm SR}^{\rm uns}(t)}{2}\frac{t^2}{(t+1)^4}. \quad (59)$$

It is interesting to remark the following. First, as seen from Eqs. (52) and (57), the strength of misfit piezoelectric and misfit deformation scatterings is specified by the difference in lattice constant and the interface roughness. As a result, the relevant partial transport and quantum lifetimes are found to quadratically decrease with an increase of the lattice mismatch $\epsilon_{\parallel}$ and the roughness amplitude Δ. Second, as seen from Eqs. (55) and (58), the form factors for these scatterings are factorized into two parts: the first one is fixed by the roughness profile $F_{\rm SR}^{\rm uns}(t)$, so by the correlation length Λ, while the second one is fixed by the features of the electron distribution and the scattering mechanism under consideration.

To end this section, we conclude that within the realistic model of finitely deep QWs described by the modified Fang-Howard wave function from Eq. (1), we have derived the autocorrelation functions in an analytic form for the diverse scattering mechanisms of interest. These are supplied by Eqs. (34), (39), (43), (52), and (57) for background impurities, alloy disorder, surface roughness, misfit piezoelectric charges, and misfit deformation potential, respectively. In difference from the earlier theories,[2,17,19] our calculation of the transport and quantum lifetimes properly involves the effects from uniform doping and exchange-correlation corrections through their effects on the quantum confinement.

IV. RESULTS AND CONCLUSIONS

A. Input parameters

In this section, we are trying to apply the preceding theory to understand the transport properties of electrons in wurtzite group-III-nitride heterostructures. In particular, we attempt to explain the recent experimental data[11] about the transport and quantum lifetimes as well as their ratio of the low-temperature high-density 2DEG in GaN as the conduction channel in background-doped strained $Al_xGa_{1-x}N/GaN$ heterojunctions.

For numerical results, we have to specify parameters appearing in the theory as input. The lattice constants, elastic stiffness constants, piezoelectric constants, and dielectric constants for AlN and GaN are taken from Refs. 27 and 58, and listed in Table I in Ref. 17. The corresponding constants for an $Al_xGa_{1-x}N$ alloy are estimated within the virtual crystal approximation.[27] The effective electron masses of GaN are for the growth direction $m_z = 0.18\ m_{\rm e}$[59] and for the in-plane $m^* = 0.228\ m_{\rm e}$.[60]

We are examining the key parameters to which the calculation of the quantum confinement, i.e., the electron distribution in $Al_xGa_{1-x}N/GaN$ heterostructures, is sensitive. First, the potential barrier height is normally assumed to be equal to the conduction band offset between the $Al_xGa_{1-x}N$ barrier and the GaN well, $V_0 = \Delta E_{\rm c}(x)$, which depends on the Al content x as[48,61,62]

$$\Delta E_{\rm c}(x) = 0.75[E_{\rm g}(x) - E_{\rm g}(0)], \quad (60)$$

where the band gap of $Al_xGa_{1-x}N$ is measured to be[27]

$$E_{\rm g}(x) = 6.13x + 3.42(1-x) - x(1-x)\ {\rm eV}. \quad (61)$$

Second, some recent experimental and theoretical investigations[28,63] suggested that the measured spontaneous polarization charge density may be much smaller than the previous theoretical estimates.[25–27,64] Aiming at the explanation of the experiment on the relaxation times, we adopt the measured value of this charge density of AlN reported in Ref. 63: $\sigma_{\rm sp}({\rm AlN}) = -0.040\ {\rm C/m^2}$. Then, the total density of sheet polarization charges is given as a function of the Al content by

$$\sigma(x) = 0.011x - 2\frac{a(x)-a(0)}{a(0)}\left[e_{31}(x) - e_{33}(x)\frac{c_{13}(x)}{c_{33}(x)}\right] \quad (62)$$

(in units of ${\rm C/m^2}$).

B. Quantum confinement effect due to uniform doping in infinitely deep QWs

For an apparent illustration of the effect of uniform doping on the quantum confinement, we have calculated it in the limiting case of infinitely deep QWs, ignoring provisionally the penetration of the 2DEG into the barrier layer and their exchange-correlation corrections. These are both included in the subsequent calculation with reference to the experiment.

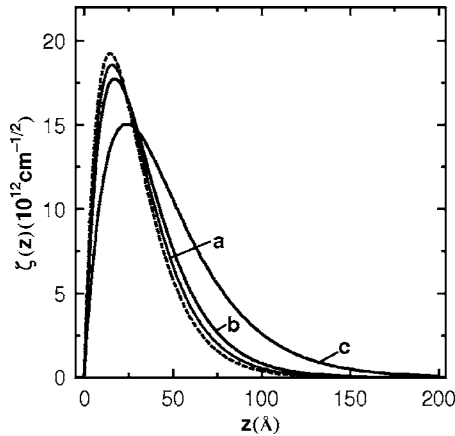

FIG. 1. Standard Fang-Howard wave function $\zeta(z)$ along the growth direction in the presence (solid lines) and the absence (dashed one) of uniform doping. The solid lines labeled a, b, and c correspond to different doping capacities $N_I z_w = 1\times 10^{12}$, 2×10^{12}, and 4×10^{12} cm^{-2}, respectively.

In Fig. 1, we display the standard Fang-Howard wave functions along the growth direction with and without uniform doping, by employing Eq. (26) for the well wave number. These are plotted for an $Al_xGa_{1-x}N/GaN$ sample of $x=0.23$, a total sheet polarization charge density $\sigma/e=6.93\times 10^{12}$ cm^{-2}, under a sheet carrier density $n_s=5\times 10^{12}$ cm^{-2} and different doping capacities $N_I z_w = 1\times 10^{12}$, 2×10^{12}, and 4×10^{12} cm^{-2}.

The dependence of a scattering event on the momentum transfer, or equivalently, its angular distribution is evidently described completely by the form factor for the screened scattering, defined by

$$F^{\rm scr}(t) = F^{\rm uns}(t)/\varepsilon^2(t), \tag{63}$$

where $F^{\rm uns}(t)$ is the form factor for the relevant unscreened scattering. The dielectric function is rewritten in terms of the dimensionless variables $t=q/k$ and $t_s=q_s/k$:

$$\varepsilon(t) = 1 + \frac{t_s}{t}F_S(t)[1-G(t)], \quad \text{for } t \leqslant 2t_F, \tag{64}$$

where $F_S(t)$ and $G(t)$ are, as before, given by Eqs. (31) and (32).

As seen from Eq. (51), in the limiting case of interface profiles with a very short (zero) correlation length one has simply[12] $F_{SR}(t)|_{\Lambda=0}=1$, so that it holds for the form factor for the screened surface roughness scattering from a δ-correlated interface,

$$F_{SR}^{\rm scr}(t)|_{\Lambda=0} = 1/\varepsilon^2(t). \tag{65}$$

This means that in this case the angular distribution of the screened surface roughness scattering coincides with the one of the screening.

The screened $F^{\rm scr}(t)$ and unscreened $F^{\rm uns}(t)$ form factors are plotted versus the dimensionless momentum transfer t in units of $2t_F$ (and scattering angle θ) in Fig. 2 for various scattering mechanisms. The unscreened form factors for background impurities, surface roughness, misfit piezoelectric charges, and misfit deformation potential are supplied by Eqs. (35), (51), (56), and (59), respectively. The ionic correlation effect is estimated at a doping level $N_I=5\times 10^{16}$ cm^{-3}, and the dimensionless correlation length is set at $\Lambda k=0,1,5$.

In order to illustrate the influence from the doping-related quantum confinement on the above-quoted scattering sources, we calculate the relaxation times of the $Al_{0.23}GaN_{0.77}$ (210 Å)/GaN (4.7 μm) heterojunction studied in Ref. 11 in the limiting case of infinitely deep QWs. At $x=0.23$ the lattice mismatch is $\epsilon_\parallel=0.56\%$. The transport τ^t and quantum τ^q lifetimes are depicted against the impurity density ranging from $N_I=1\times 10^{15}-1\times 10^{16}$ cm^{-3} in Fig. 3, where the sheet carrier density is set at $n_s=5\times 10^{12}$ cm^{-2}, the interface profile is with a roughness amplitude $\Delta=3$ Å and correlation length $\Lambda=10$ and 100 Å. The lifetime ratio τ^t/τ^q due to impurity scattering is given in the inset in Fig. 3(a) as a function of the doping level, while those due to roughness-induced scatterings, viz. surface roughness, piezoelectric, and deformation potentials, are shown in Fig. 4 as a function of the correlation length.

From the lines thus obtained, we may draw the following conclusions.

(i) As evidently seen from Fig. 1, because of uniform doping with positive donors the centroid of the electron distribution is to be shifted toward the well side. The effect is increased rather rapidly with the doping capacity, namely, the shift is $\Delta z_0=1.6$, 3.9, and 14.0 Å for $N_I z_w=1\times 10^{12}$, 2×10^{12}, and 4×10^{12} cm^{-2}, respectively.

(ii) It follows from Fig. 2(a) that the ionic correlation among charged impurities leads to a significant reduction of their scattering. Consequently, the form factor for the screened scattering by correlated impurities is found to be more isotropic, i.e., not limited only at small angles (forward scattering) as in the case of random impurities.

(iii) An examination of the dashed lines in Figs. 2(b)–2(d) reveals that with a rise of the correlation length all unscreened roughness-induced scatterings are remarkably reduced. The reduction at large angles is greater than at small ones. For very short correlation length ($\Lambda=0$), the surface roughness scattering is isotropic, and the misfit deformation potential one occurs in almost all angles except for $\theta\sim 0$, while the misfit piezoelectric one occurs mainly in narrower angles ($\theta\lesssim \pi/3$).

(iv) As observed from Eqs. (28) and (29), the effect of screening on the relaxation times is described completely by the quantity $1/\varepsilon^2(t)$. In accordance with Eq. (65), this is shown as a function of the momentum transfer by the solid line with label $\Lambda k=0$ in Fig. 2(b). The screening effect is seen to be anisotropic, especially very strong at small angles, i.e., forward scattering. Therefore, the screened scattering is reduced strongly at small angles, so that the peak in its angular distribution is shifted toward large angles. Moreover, a comparison of the solid lines in each of Figs. 2(b)–2(d) reveals that with increasing correlation length the peak in the angular distribution of screened SR, PE, and DP scatterings is shifted toward small angles, i.e., forward scattering as in case of Coulomb scattering by random impurities.

(v) An inspection of Fig. 3(a) indicates that when raising the doping level the relevant transport and quantum lifetimes

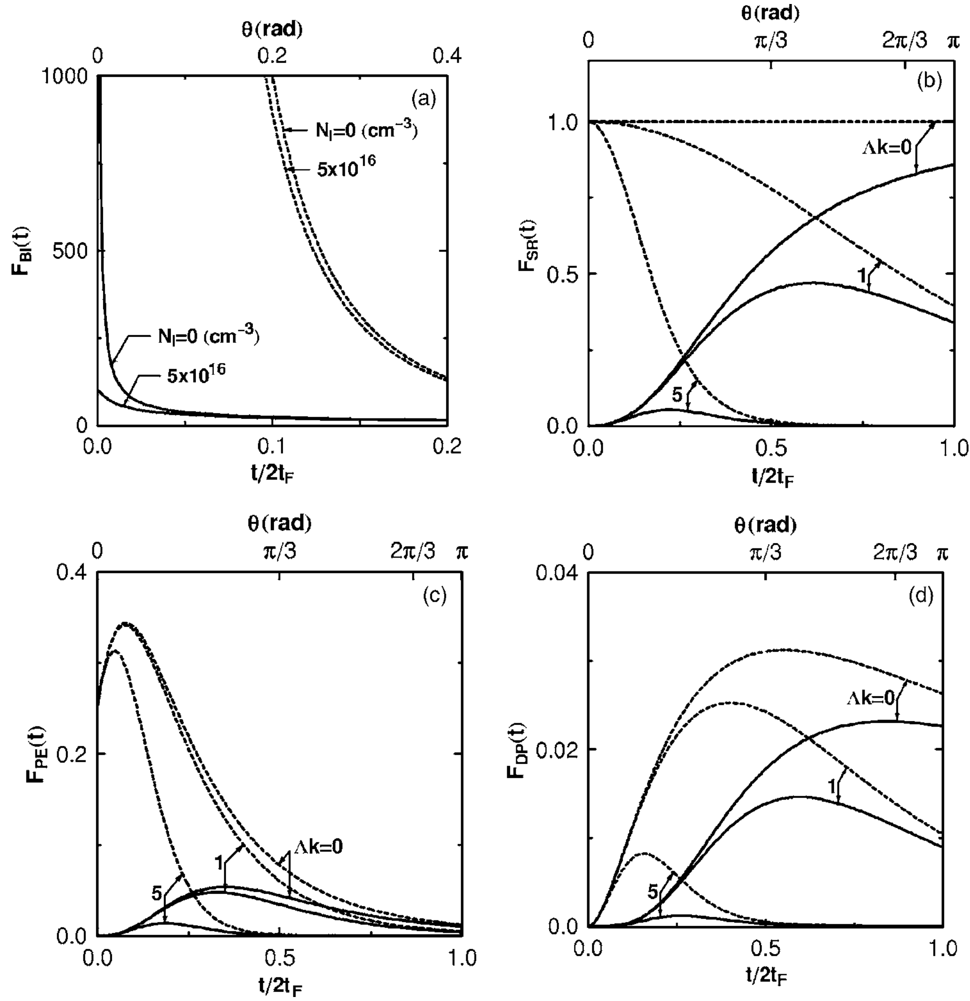

FIG. 2. Screened $F^{scr}(t)$ and unscreened $F^{uns}(t)$ form factors vs dimensionless momentum transfer t in units of $2t_F$ (and scattering angle θ) for different scattering mechanisms in an infinitely deep QW: (a) background impurities (BI), (b) surface roughness (SR), (c) misfit piezoelectric charges (PE), and (d) misfit deformation potential (DP). The solid and dashed lines refer to the screened and unscreened form factors, respectively.

are significantly decreased, which is clearly connected with enhanced BI scattering. The lifetime ratio due to correlated impurities is found to weakly depend on the doping level at the used levels $\tau_{BI}^t/\tau_{BI}^q \sim 5-6$. Thus, the lifetime ratio due to correlated impurities is much smaller than that due to random impurities (more than 100 in some cases),[1,10] which is connected with the more isotropic angular distribution of scattering by the former as quoted above.

(vi) Figures 3(b)–3(d) also reveal that the relaxation times due to roughness-induced scatterings are increased when raising the doping level, which is associated with an enhanced shift of the electron distribution far away from the scattering sources located near the interface such as surface roughness, misfit piezoelectric, and deformation potentials.

(vii) It follows from Fig. 4 that with a rise of the correlation length the lifetime ratios due to roughness-induced scatterings are elevated, which is, as quoted above, associated with the shift of their angular distribution toward small angles. Consequently, these ratios can become much larger than unity. For instance, for all SR, PE, and DP scatterings, we observe at $\Lambda=10$ Å $\tau^t/\tau^q \sim 1$; however, at $\Lambda=200$ Å, $\tau_{DP}^t/\tau_{DP}^q \sim 15$ and $\tau_{SR}^t/\tau_{SR}^q \approx \tau_{PE}^t/\tau_{PE}^q \sim 25$. This result is different from the earlier argument[1,65] that the transport and quantum lifetimes due to surface roughness are the same. Moreover, we find for $\Lambda \lesssim 400$ Å, $\tau_{SR}^t/\tau_{SR}^q \approx \tau_{PE}^t/\tau_{PE}^q$. This means that in difference from the earlier belief[8] the value of the lifetime ratio should not be used as a tool to recognize the scattering mechanism.

C. Numerical results for finitely deep QWs and comparison with experiment

To end this section, we are dealing with the observed data about the electron density dependencies of the transport and quantum lifetimes as well as their ratio in a biased $Al_{0.23}Ga_{0.77}N$ (210 Å)/GaN (4.7 μm) single heterostructure reported in Ref. 11. The numerical self-consistent calculation pointed out[3,48,66] that the confining potential of such a system is basically of a triangular QW shape, especially in the well region, where the electrons are mainly concentrated, so that we may adopt the modified Fang-Howard wave function to describe approximately the 2DEG of interest. Therefore, we

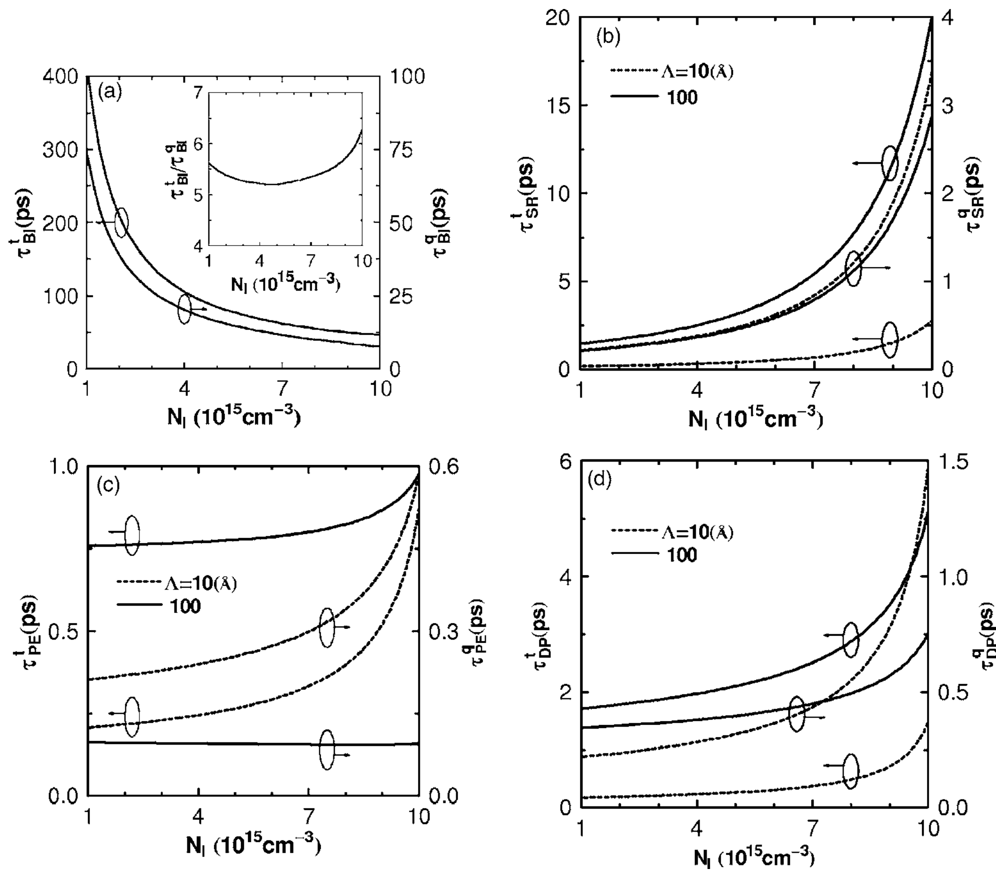

FIG. 3. Transport τ^t and quantum τ^q lifetimes due to BI, SR, PE, and DP scatterings for the 2DEG in an $Al_{0.23}Ga_{0.77}N/GaN$ heterojunction of an infinitely high potential barrier vs impurity density N_I. The left-hand and right-hand axis refers to the transport and quantum lifetimes, respectively.

may apply the foregoing theory to the sample under study.

For quantitative explanation, we have carried out the calculation for the realistic sample, allowing for the effects from both the finiteness of the potential barrier height and the exchange-correlation corrections. At the Al content $x=0.23$, the barrier height is $V_0=0.335$ eV. The doping level is set at $N_I=4.5\times10^{15}$ cm^{-3}. It was shown[13,55] that the most important component of the interface roughness is connected with elastic strain relaxation in the channel layer, and its correlation length is such that $\Lambda\lesssim300$ Å. So, the interface profile is to be chosen with a roughness amplitude $\Delta=2.7$ Å and a correlation length $\Lambda=265$ Å.

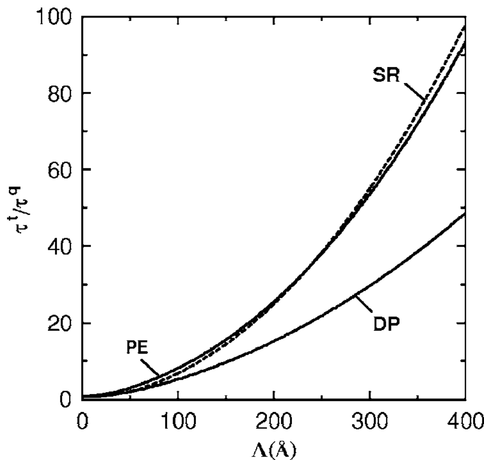

FIG. 4. Transport-to-quantum-lifetime ratio τ^t/τ^q due to SR, PE, and DP scatterings for the 2DEG in an $Al_{0.23}Ga_{0.77}N/GaN$ heterojunction of an infinitely high potential barrier vs correlation length Λ.

In accordance with the estimation presented in Fig. 3(a), at the used doping level the scattering from correlated background impurities is very weak, yielding the lifetimes much (two order of magnitude) larger than the measured ones, so it is neglected. Further, the evaluation of the scattering by independent charged dislocations with a density of 7.8×10^8 cm^{-2} supplied[11,67] the transport lifetime at least three times larger than the measured one. As mentioned before, the scattering by interacting dislocations seems to be remarkably weaker than that by the independent ones. Consequently, the transport lifetime limited by interacting dislocations must be at least one order of magnitude larger than the measured one. This implies that in this case the dislocation scattering is so weak that it may be ignored.

Thus, the individual and overall 2DEG transport and quantum lifetimes and their ratio due to AD, SR, PE, and DP scatterings are plotted versus the electron density varying from $n_s=2\times10^{12}-10\times10^{12}$ cm^{-2} in Figs. 5–7, where the 4.2 K measured data[11] are also reproduced for comparison.

From the lines thus obtained, we may draw the following conclusions.

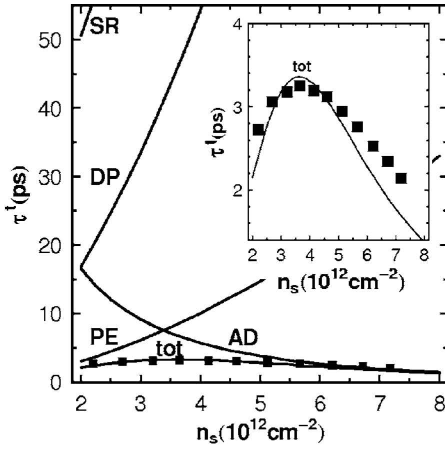

FIG. 5. Transport lifetime τ^t for an $Al_{0.23}Ga_{0.77}N$ (210 Å)/GaN (4.7 μm) sample vs sheet electron density n_s. The 4.2 K experimental data (Ref. 11) are marked by squares.

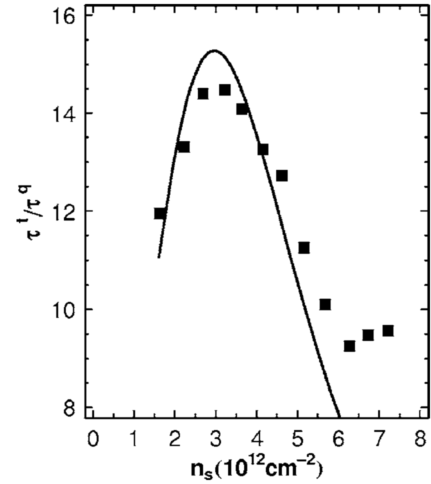

FIG. 7. Transport-to-quantum-lifetime ratio τ^t/τ^q for an $Al_{0.23}Ga_{0.77}N$ (210 Å)/GaN (4.7 μm) sample vs sheet electron density n_s. The 4.2 K experimental data (Ref. 11) are marked by squares.

(i) The relaxation times provided by our theory are found to be in a good agreement with the experimental data[11] on the sample under study. The calculated transport lifetime almost coincides with the measured one in the carrier density regime in use. The peaks of the theoretical and experimental curves are found to be located at nearly the same density $n_s=3.6\times10^{12}$ cm^{-2} with a nearly equal height: $\tau^t_{\rm theor}=3.36$ ps and $\tau^t_{\rm expt}=3.25$ ps. The situation with the quantum lifetime is not as good as with the transport one. The theory shows a peak of the quantum lifetime $\tau^q_{\rm theor}=0.31$ ps at $n_s=8.6\times10^{12}$ cm^{-2}, which is somewhat larger than the observed one, $\tau^q_{\rm expt}=0.27$ ps at $n_s=6\times10^{12}$ cm^{-2}.

It is to be recalled that the transport lifetime of the 2DEG in the uniformly doped sample here is large compared to that in the modulation-doped one addressed in Ref. 12. The why is that in the former the electron distribution is shifted far away from the interface, so the scattering weakened, whereas in the latter is shifted in the opposite direction, so the scattering strengthened.

(ii) As evidently seen from Fig. 7, the calculated ratio of the total lifetimes can well reproduce the measured one, both in the bell shape and the magnitude. The peaks of the theoretical and experimental curves are found to be located at the same density $n_s=3\times10^{12}$ cm^{-2} with a nearly equal height: $\tau^t_{\rm theor}/\tau^q_{\rm theor}=15.3$ and $\tau^t_{\rm expt}/\tau^q_{\rm expt}=14.6$, while the peak predicted by the earlier theory[2] is two times larger than that measured.

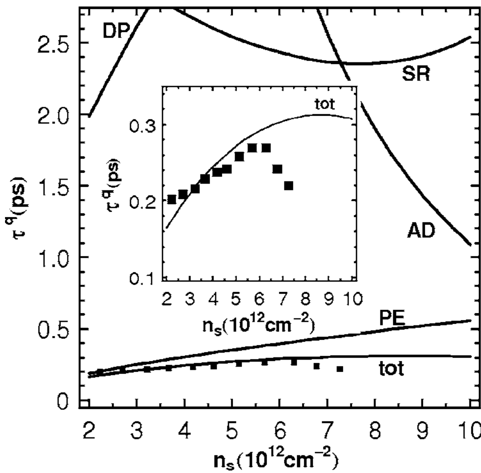

FIG. 6. Quantum lifetime τ^q for an $Al_{0.23}Ga_{0.77}N$ (210 Å)/GaN (4.7 μm) sample vs sheet electron density n_s. The 4.2 K experimental data (Ref. 11) are marked by squares.

(iii) An examination of Figs. 5 and 6 reveals that surface roughness and misfit deformation potential scatterings are less important in limiting the measured transport and quantum lifetimes. These are both dominated by misfit piezoelectric and alloy disorder scatterings. The former is responsible for the increasing tendency at small carrier densities, whereas the latter for the decreasing tendency at large densities, so producing the peaks detected in the lifetime curves. This bell shape is in sharp contrast to the concave shape of the quantum lifetime predicted by the earlier theory[2] based only on the well-known scattering sources.

V. SUMMARY

To summarize, in the present paper we have developed a comprehensive theory for the transport and quantum lifetimes of the 2DEG at low temperature and high carrier density in uniformly doped wurtzite group-III-nitride heterostructures. Besides the traditional scattering sources, we incorporated in the calculation the roughness-induced scatterings: misfit piezoelectric charges and misfit deformation potential. Moreover, we included the quantum confinement due to uniform doping.

The effect of uniform doping is twofold: a scattering source for the 2DEG in the in-plane, but also a confining source in the growth direction. At low doping levels the former is found to be negligibly weak, while the latter is an important factor, which via quantum confinement suppresses the other scattering mechanisms.

The roughness-related scattering mechanisms such as surface roughness, misfit piezoelectric, and deformation poten-

tials can be a short- or long-range process depending on the correlation length of the interface profile, so that their lifetime ratios can become much larger than unity.

In contrast to the previous calculation starting merely from the so-far known scattering sources, our theory turns out to enable a satisfactory description of the recent experimental data[11] in a high 2DEG density regime about both the relaxation times. The theory is found in a very good quantitative agreement with the measured transport lifetime and lifetime ratio, while the agreement with the measured quantum lifetime is somewhat good.

The roughness-induced scatterings are found to be key sources in determining the carrier density dependencies of the transport and quantum lifetimes. In particular, misfit piezoelectric scattering is responsible for the increasing tendency, whereas alloy disorder is responsible for the decreasing one, and produces the bell shapes observed in the lifetimes and their ratio.

The ionic correlation is proven to be important in the linear transport theory for uniform doping scattering because this warrants the convergence of the integral representing the inverse quantum lifetime. As a result, this quantum lifetime becomes nonvanishing, so that the lifetime ratio due to scattering by correlated impurities is much smaller than that by random ones. Furthermore, we suggest that the interactions among dislocations might reduce significantly their scattering so that the divergence of the inverse quantum lifetime due to charged dislocations is eliminated with an inclusion of their interactions.

We also indicate that the value of the lifetime ratio should not be used as a tool to recognize the scattering mechanism.

[1] S. Das Sarma and F. Stern, Phys. Rev. B **32**, 8442 (1985).

[2] L. Hsu and W. Walukiewicz, Appl. Phys. Lett. **80**, 2508 (2002).

[3] N. Maeda, T. Saitoh, K. Tsubaki, T. Nishida, and N. Kobayashi, Appl. Phys. Lett. **76**, 3118 (2000).

[4] P. T. Coleridge, R. Stoner, and R. Fletcher, Phys. Rev. B **39**, 1120 (1989).

[5] J. J. Harris, K. J. Lee, T. Wang, S. Sakai, Z. Bougrioua, I. Moerman, E. J. Thrush, J. B. Webb, H. Tang, T. Martin, D. K. Maude, and J-C. Portal, Semicond. Sci. Technol. **16**, 402 (2001).

[6] M. J. Manfra, S. H. Simon, K. W. Baldwin, A. M. Sergent, K. W. West, R. J. Molnar, and J. Caissie, Appl. Phys. Lett. **85**, 5278 (2004).

[7] J. M. Manfra, L. N. Pfeiffer, K. W. West, H. L. Stormer, K. W. Baldin, J. W. P. Hsu, D. V. Lang, and R. J. Molnar, Appl. Phys. Lett. **77**, 2888 (2000).

[8] S. Elhamri, A. Saxler, W. C. Mitchel, C. R. Elsass, I. P. Smorchkova, B. Heying, E. Haus, P. Fini, J. P. Ibbetson, S. Keller, P. M. Petroff, S. P. DenBaars, U. K. Mishra, and J. S. Speck, J. Appl. Phys. **88**, 6583 (2000).

[9] A. Link, T. Graf, R. Dimitrov, O. Ambacher, M. Stutzmann, Y. Smorchkova, U. Mishra, and J. Speck, Phys. Status Solidi B **228**, 603 (2001).

[10] D. Jena and U. K. Mishra, Phys. Rev. B **66**, 241307(R) (2002).

[11] P. Lorenzini, Z. Bougrioua, A. Tiberj, R. Tauk, M. Azize, M. Sakowicz, K. Karpierz, and W. Knap, Appl. Phys. Lett. **87**, 232107 (2005).

[12] J. Antoszewski, M. Gracey, J. M. Dell, L. Faraone, T. A. Fisher, G. Paris, Y.-F. Wu, and U. K. Mishra, J. Appl. Phys. **87**, 3900 (2000).

[13] R. M. Feenstra and M. A. Lutz, J. Appl. Phys. **78**, 6091 (1995).

[14] D. N. Quang, V. N. Tuoc, N. H. Tung, and T. D. Huan, Phys. Rev. Lett. **89**, 077601 (2002); Phys. Rev. B **68**, 153306 (2003).

[15] D. N. Quang, N. H. Tung, V. N. Tuoc, N. V. Minh, and P. N. Phong, Phys. Rev. B **72**, 115337 (2005).

[16] D. N. Quang, V. N. Tuoc, T. D. Huan, and P. N. Phong, Phys. Rev. B **70**, 195336 (2004).

[17] D. N. Quang, V. N. Tuoc, N. H. Tung, N. V. Minh, and P. N. Phong, Phys. Rev. B **72**, 245303 (2005).

[18] T. Ando, A. B. Fowler, and F. Stern, Rev. Mod. Phys. **54**, 437 (1982).

[19] L. Hsu and W. Walukiewicz, Phys. Rev. B **56**, 1520 (1997); Appl. Phys. Lett. **73**, 339 (1998).

[20] T. Ando, J. Phys. Soc. Jpn. **51**, 3893 (1982); **51**, 3900 (1982).

[21] G. Bastard, *Wave Mechanics Applied to Semiconductor Heterostructures* (Les Editions de Physique, Paris, 1988).

[22] Y. Okuyama and N. Tokuda, Phys. Rev. B **40**, 9744 (1989).

[23] T.-H. Yu and K. F. Brennan, J. Appl. Phys. **89**, 3827 (2001).

[24] A. Bykhovski, G. Gelmont, and M. Shur, J. Appl. Phys. **74**, 6734 (1993).

[25] F. Bernardini, V. Fiorentini, and D. Vanderbilt, Phys. Rev. B **56**, R10024 (1997).

[26] I. P. Smorchkova, C. R. Elsass, J. P. Ibbetson, R. Vetury, B. Heying, P. Fini, E. Haus, S. DenBaars, J. S. Spect, and U. K. Mishra, J. Appl. Phys. **86**, 4520 (1999).

[27] O. Ambacher, B. Foutz, J. Smart, J. R. Shealy, N. G. Weimann, K. Chu, M. Murphy, A. J. Sierakowski, W. J. Shaff, L. F. Eastman, R. Dimitrov, A. Mitchell, and M. Stutzmann, J. Appl. Phys. **87**, 334 (2000).

[28] L. Hsu and W. Walukiewicz, J. Appl. Phys. **89**, 1783 (2001).

[29] R. Enderlein and N. J. M. Horing, *Fundamentals of Semiconductor Physics and Devices* (World Scientific, Singapore, 1997).

[30] W. Kohn and L. J. Sham, Phys. Rev. **140**, A1133 (1965).

[31] P. Ruden and G. H. Döhler, Phys. Rev. B **27**, 3538 (1983).

[32] I. S. Gradshteyn and I. M. Ryzhik, *Table of Integrals, Series, and Products*, 4th ed. (Academic, New York, 1980).

[33] A. Gold and W. Götze, J. Phys. C **14**, 4049 (1981); Phys. Rev. B **33**, 2495 (1986).

[34] F. Stern and W. E. Howard, Phys. Rev. **163**, 816 (1967).

[35] A. Gold, Phys. Rev. B **35**, 723 (1987).

[36] M. Jonson, J. Phys. C **9**, 3055 (1976).

[37] W. Walukiewicz, H. E. Ruda, J. Lagowski, and H. C. Gatos, Phys. Rev. B **30**, 4571 (1984).

[38] E. F. Schubert, J. E. Cunningham, and N. T. Tsang, Solid State Commun. **63**, 591 (1987).

[39] E. F. Schubert, J. M. Kuo, R. F. Kopf, H. S. Luftman, L. C. Hopkins, and N. J. Sauer, J. Appl. Phys. **67**, 1969 (1990).

[40] A. L. Efros, F. G. Pikus, and G. G. Samsonidze, Phys. Rev. B **41**, 8295 (1990).

[41] D. N. Quang, N. N. Dat, and D. V. An, Phys. Lett. A **182**, 125 (1993).
[42] D. N. Quang and N. H. Tung, Phys. Status Solidi B **207**, 111 (1998).
[43] A. Gold, Phys. Rev. B **38**, 10798 (1988).
[44] J. P. Harrang, R. J. Higgins, R. K. Goodall, P. R. Jay, M. Laviron, and P. Delescluse, Phys. Rev. B **32**, 8126 (1985).
[45] P. T. Coleridge, Phys. Rev. B **44**, 3793 (1991).
[46] A. Fischer, H. Kuhne, and H. Richter, Phys. Rev. Lett. **73**, 2712 (1994).
[47] D. Jena, Y. P. Smorchkova, C. R. Elsass, A. C. Gossard, and U. K. Mishra, in Proceedings of the 25th International Conference on Physics of Semiconductors, Osaka, 2000, Springer Proceedings in Physics Vol. 87, edited by N. Miura and T. Ando (Springer, Berlin, 2001), p. 771.
[48] N. Maeda, T. Nishida, N. Kobayashi, and M. Tomizawa, Appl. Phys. Lett. **73**, 1856 (1998).
[49] D. Jena, S. Heikman, J. S. Speck, A. Gossard, U. K. Mishra, A. Link, and O. Ambacher, Phys. Rev. B **67**, 153306 (2003).
[50] S. Rajan, S. P. DenBaars, U. Mishra, H. Xing, and D. Yena, Appl. Phys. Lett. **88**, 042103 (2006).
[51] J. Simon, A. Wang, H. Xing, S. Rajan, and D. Jena, Appl. Phys. Lett. **88**, 042109 (2006).
[52] F. M. S. Lima, Q. Fanyao, O. A. C. Nunes, and A. L. A. Fonseca, Phys. Status Solidi B **225**, 43 (2001).
[53] F. M. S. Lima, A. L. A. Fonseca, O. A. C. Nunes, and Q. Fanyao, J. Appl. Phys. **92**, 5296 (2002).
[54] T. Ando, J. Phys. Soc. Jpn. **43**, 1616 (1977).
[55] R. M. Feenstra, M. A. Lutz, F. Stern, K. Ismail, P. M. Mooney, F. K. LeGoues, C. Stanis, J. O. Chu, and B. S. Meyerson, J. Vac. Sci. Technol. B **13**, 1608 (1995).
[56] S. Chichibu, A. Shikanai, T. Azuhata, T. Sota, A. Kuramata, K. Horino, and S. Nakamura, Appl. Phys. Lett. **68**, 3766 (1996).
[57] A. Shikanai, T. Azuhata, T. Sota, S. Chichibu, A. Kuramata, K. Horino, and S. Nakamura, J. Appl. Phys. **81**, 417 (1997).
[58] K. Kim, W. R. L. Lambrecht, and B. Segall, Phys. Rev. B **53**, 16 310 (1996).
[59] M. Suzuki, T. Uenoyama, and A. Yanase, Phys. Rev. B **52**, 8132 (1995).
[60] L. W. Wong, S. J. Cai, R. Li, K. Wang, H. W. Jiang, and M. Chen, Appl. Phys. Lett. **73**, 1391 (1998).
[61] G. Martin, S. Strite, A. Botchkarev, A. Agarwal, A. Rockett, H. Morkoç, W. R. L. Lambrecht, and B. Segall, Appl. Phys. Lett. **65**, 610 (1994).
[62] G. Martin, A. Botchkarev, A. Rockett, and H. Morkoç, Appl. Phys. Lett. **68**, 2541 (1996).
[63] S.-H. Park and S.-L. Chuang, Appl. Phys. Lett. **76**, 1981 (2000).
[64] K. Shimada, T. Sota, and K. Suzuki, J. Appl. Phys. **84**, 4951 (1998).
[65] Z. W. Zheng, B. Shen, C. P. Jiang, Y. S. Gui, T. Someya, R. Zhang, Y. Shi, Y. D. Zheng, S. L. Guo, J. H. Chu, and Y. Arakawa, J. Appl. Phys. **93**, 1651 (2003).
[66] B. Vinter, in *Heterojunctions and Semiconductor Superlattices*, edited by G. Allan, G. Bastard, N. Boccara, M. Lannoo, and M. Voos (Springer, Berlin, 1986), p. 238.
[67] M. N. Gurusinghe, S. K. Davidsson, and T. G. Andersson, Phys. Rev. B **72**, 045316 (2005).